Combustion and Flame 156 (2009) 494–504

Contents lists available at ScienceDirect

Combustion and Flame

www.elsevier.com/locate/combustflame

The combustion chemistry of a fuel tracer: Measured flame speeds and ignition delays and a detailed chemical kinetic model for the oxidation of acetone

S. Pichon [a], G. Black [a], N. Chaumeix [b], M. Yahyaoui [b], J.M. Simmie [a,*], H.J. Curran [a], R. Donohue [c]

[a] Combustion Chemistry Centre, National University of Ireland, Galway, Ireland
[b] Institut de Combustion Aérothermique Réactivité et Environnement, CNRS, Orléans, France
[c] Information Technology, National University of Ireland, Galway, Ireland

ARTICLE INFO

Article history:
Received 13 May 2008
Received in revised form 15 September 2008
Accepted 7 October 2008
Available online 14 November 2008

Keywords:
Fuel tracer
Acetone
Modelling
Ignition delay
Flame speed
Ketene

ABSTRACT

Acetone ignition delay and stretch-free laminar flame speed measurements have been carried out and a kinetic model has been developed to simulate these and literature data for acetone and for ketene, which was found to be an important intermediate in its oxidation. The mechanism has been based on one originally devised for dimethyl ether and modified through validation of the hydrogen, carbon monoxide and methane sub-mechanisms. Acetone oxidation in argon was studied behind reflected shock waves in the temperature range 1340–1930 K, at 1 atm and at equivalence ratios of 0.5, 1 and 2; it is also shown that the addition of up to 15% acetone to a stoichiometric *n*-heptane mixture has no effect on the measured ignition delay times. Flame speeds at 298 K and 1 atm of pure acetone in air were measured in a spherical bomb; a maximum flame speed of ~35 cm s^{-1} at $\phi = 1.15$ is indicated.

1. Introduction

Laser induced fluorescence (LIF) imaging is a non-invasive technique that can be applied to combustion systems as a means of monitoring the behaviour of the fuel in terms of its distribution, concentration and temperature [1–9]. However, many fuels either do not themselves absorb at the wavelengths normally used to induce fluorescence or if they do so, only fluoresce weakly.

Consequently, fuel tracers have come into use. These are compounds with well characterised spectral behaviour, which absorb and fluoresce at conveniently accessible wavelengths and are therefore added to a fuel in order to facilitate LIF imaging [10–13].

Acetone, aside from its role as an intermediate in the combustion of hydrocarbons and oxygenates, is important to the field of combustion as a fuel tracer [14–16]. It absorbs in a suitable wavelength range (225–320 nm), due to the spin-allowed but orbital-forbidden $\pi^* \leftarrow n$ electronic transition of the carbonyl group. In addition, its high vapour pressure makes it useful for seeding gaseous flows in the quantities required (typically 10–15%) to ensure a strong fluorescence signal. However, little is known of its chemical fate in a hot oxidising environment and therefore of its useful lifetime as a tracer in combustion conditions.

Acetone also plays an important role in atmospheric chemistry as it, and other ketones, are produced through the radical oxidation of hydrocarbons in the atmosphere [17,18]. Indeed acetone is the most abundant oxygenated organic in the upper troposphere [19]. The uncontrolled burning of household waste is also known to lead to the formation of acetone with subsequent release into the atmosphere [20]. An understanding of the kinetics of the oxidation of acetone, and radicals derived from it [21], is therefore important to both atmospheric and combustion chemistry.

Acetone oxidation in the gas-phase has been studied by Hoare et al. [22–24] and also Barnard and Honeyman [25,26]. Barnard and Honeyman proposed that the most plausible chain-initiating step was the attack on acetone by oxygen via $CH_3COCH_3 + O_2 \rightarrow CH_3C\dot{O}CH_2 + H\dot{O}_2$. Then, the acetonyl radical decomposed by breaking a C–C bond to give a methyl radical and ketene $CH_3C\dot{O}CH_2 \rightarrow \dot{C}H_3 + CH_2CO$. Methyl radical may react in two ways depending on the temperature. At temperatures below about 720 K, the reaction is termolecular and ultimately results in the production of methyl hydroperoxide:

$$\dot{C}H_3 + O_2 + M \rightarrow CH_3O\dot{O} + M,$$

$$CH_3O\dot{O} + RH \rightarrow CH_3OOH + \dot{R},$$

$$CH_3O\dot{O} + CH_3 \rightarrow CH_3\dot{O} + CH_3\dot{O},$$

whereas at high temperatures the reaction is bimolecular:

$$\dot{C}H_3 + O_2 \rightarrow HCHO + \dot{O}H.$$

* Corresponding author.
E-mail address: john.simmie@nuigalway.ie (J.M. Simmie).
URL: http://c3.nuigalway.ie/ (J.M. Simmie).

0010-2180/$ – see front matter
doi:10.1016/j.combustflame.2008.10.001

Tsuboi et al. [27] studied the thermal oxidation and decomposition of acetone behind reflected shock waves in the temperature range 1240–1620 K, using UV absorption and IR emission diagnostics. They proposed an acetone oxidation mechanism which includes the following main pathways:

$$(CH_3)_2CO \rightsquigarrow CH_3\dot{C}O \rightsquigarrow \dot{C}H_3 \rightsquigarrow C_2H_6 \rightsquigarrow C_2H_4 \rightsquigarrow H_2CO \rightsquigarrow CO \rightsquigarrow CO_2.$$

Acetone may undergo pyrolysis, hydrogen abstraction leading to the formation of ketene via the acetonyl radical [28], reaction with hydroxyl or hydrogen radicals to form acetaldehyde or reaction with an oxygen atom to give the acetyl radical.

Sato and Hidaka [29] studied the oxidation and pyrolysis of acetone behind reflected shock waves using UV absorption and IR absorption and emission diagnostics, in the temperature range 1050–1650 K, at pressures between 1.2 and 3.2 atm and in the equivalence ratio range 0.5–2. They developed a mechanism consisting of 164 reactions and 51 species.

Chaos et al. [30] studied acetone oxidation in a variable pressure flow reactor at high pressure (12.5 atm), and a temperature of 960 K for a range of stoichiometries (0.6, 1 and 1.6) and an initial fuel concentration of 1800 ppm. They measured the time histories of stable species concentrations such as CH_3COCH_3, O_2, CO, CH_4, C_2H_2, C_2H_4 and C_2H_6 and developed a kinetic model consisting of 248 reactions and 46 species.

In a very recent comprehensive study of low-pressure premixed C3 oxygenated hydrocarbon flames Li et al. [31] measured species profiles by the very powerful technique of molecular-beam mass spectrometry, with tunable synchroton radiation in the vacuum ultraviolet used to selectively photoionise each species. Some twenty six combustion intermediates, including five radicals, were detected in the lean ($\phi = 0.76$) acetone flame and rather more in the rich ($\phi = 1.83$) flame—this data is extremely valuable for the purposes of mechanism validation.

Gibbs and Calcote [32], investigating the influence of structure on burning velocity, measured the flame speeds of various compounds, including acetone, at 298 K in air, using the burner method. For acetone, they measured a maximum flame speed of 44.4 cm s^{-1} at an equivalence ratio of 0.93.

2. Experimental

2.1. Shock tube

Ignition delay measurements were carried out in a shock tube consisting of a test section measuring 6.22 m in length, with an internal diameter of 10.24 cm, and a barrel-shaped driver section measuring 53 cm in length. The two sections were separated by a polycarbonate diaphragm, which burst when forced into contact with a cross-shaped cutter due to the pressure differential between the high pressure driver section and the low pressure test section. The driver gas used was helium (99.99% pure; BOC).

Four pressure transducers located along the last half metre of the tube were used to determine the velocity of the incident shock wave. The velocity at the endwall was determined through linear extrapolation, so as to take attenuation of the shock wave into account. This value was then used to calculate the temperature and pressure of the mixture behind the reflected shock wave using the equilibrium program Gaseq [33].

The pressure at the endwall was monitored by means of an in situ pressure transducer (Kistler, model 603B). Light emission from CH* at 431 nm was detected through a fused silica window embedded in the endplate using a photodetector (Thorlabs Inc. PDA55-EC) and a narrow band-pass filter centred at 430 nm with a full-width half-maximum of 10 nm.

The ignition delay time was defined as the interval between the rise in pressure due to the arrival of the shock wave at the endwall and the maximum rate of rise of the emission signal. The shock tube was validated both before and during *this work* by the very favourable agreement obtained between measured ignition delay values for *n*-heptane mixtures with others obtained previously [34,35].

Table 1
Shock tube mixture compositions in %.

Φ	Acetone	Oxygen	Argon
0.5	1.25	10.0	88.75
1.0	1.25	5.0	93.75
2.0	1.25	2.5	96.25
1.5	1.88	5.0	93.13
2.0	2.50	5.0	92.50

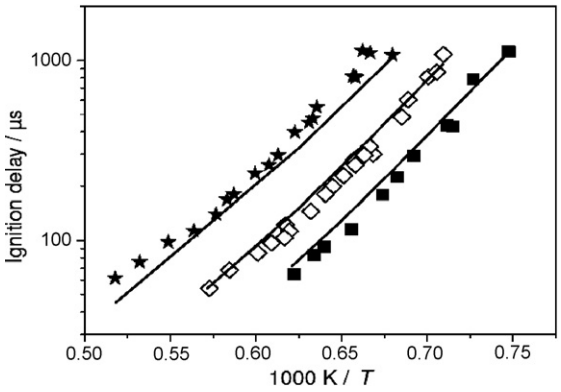

Fig. 1. Ignition delay times of acetone:O_2:Ar at fixed fuel %: (★) 1.25:2.5:96.25, (◇) 1.25:5:93.75, (■) 1.25:10:82.75, (—) simulation.

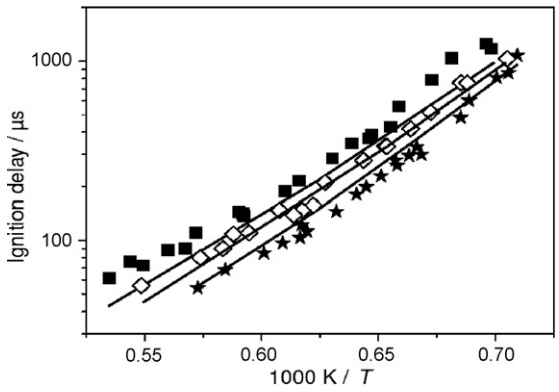

Fig. 2. Ignition delay times of acetone:O_2:Ar at fixed oxygen %: (■) 2.5:5:92.5, (◇) 1.875:5:93.125, (★) 1.25:5:93.75, (—) simulation.

The acetone (99.9% pure) was supplied by Aldrich and was degassed through a series of freeze-thaw cycles, after which no more gas was observed to escape on thawing of the solid. The oxygen (99.5% pure) and argon (99.9% pure) were supplied by BOC. Mixtures were made up using the method of partial pressures and allowed sufficient time to mix thoroughly before use, Table 1.

Ignition delay measurements were carried out in the temperature range 1340–1930 K and at a pressure of 1.02 ± 0.03 atm. Results for fixed fuel percentage are shown in Fig. 1 and for fixed oxygen percentage are shown in Fig. 2.

Our data for ignition delay times, τ, can be expressed, by least-squares multiple regression, as:

$$\tau/\mu s = 4.75 \times 10^{-7}\left[(CH_3)_2CO\right]^{0.760\pm0.065}[O_2]^{-1.269\pm0.051} \times \exp\left[(21{,}065 \pm 434)/T\right], \quad (1)$$

where the concentrations behind the reflected shock are in mol cm^{-3} and the temperature in K. The argon concentration is

virtually invariant for all the mixtures that we studied and so has not been included in the regression.

A linear regression analysis of ignition delay times measured by Sato and Hidaka [29] for their mixtures C through F yields:

$$\tau/\mu s = 5.59 \times 10^{-9}\left[(CH_3)_2CO\right]^{0.713\pm0.50}[O_2]^{-1.300\pm0.104} \times \exp\left[(25{,}279 \pm 660)/T\right]. \quad (2)$$

There is quite good agreement between the two expressions, (1) and (2), particularly as regards the acetone and oxygen power dependencies; the differences in the 'A-factors' are counterbalanced by the opposing differences in the 'activation energies' in (1) and (2) resulting in comparable ignition delay times.

Tsuboi et al. [27] quote two different correlation equations which however do include an argon power dependence; their expression for the carbon dioxide induction period:

$$\tau(CO_2) = 1.3 \times 10^{-12}\left[(CH_3)_2CO\right]^{0.29}[O_2]^{-0.53}[Ar]^{-0.25} \times \exp(19{,}970/T)$$

has a lower activation energy of 166 kJ mol^{-1} as opposed to the 175 of Eq. (1) or the 210 kJ mol^{-1} of Eq. (2).

2.2. Bomb

Flame speed measurements were carried out in a spherical bomb consisting of a stainless steel sphere with a black polished inner surface and an internal diameter of 250 mm. Two stainless steel electrodes protruded diametrically into the centre of the bomb, leaving an adjustable gap between them that typically measured about 1 mm. These electrodes were connected to a high voltage source to generate a spark between them and thereby bring about ignition in the centre of the bomb. The energy deposited by the spark was measured at 1.88 mJ.

Optical access was provided by two facing quartz windows, 70 mm in diameter and 40 mm thick. The optical system used to visualize the flame was a Schlieren set-up consisting of a xenon lamp (Jobin Yvon), a focal lens and two spherical concave mirrors (100 mm diameter, 0.5 m focal length) situated on either side of the bomb. The image was projected onto a viewing screen, where it was recorded using a high speed camera (Photron, Fastcam-ultima APX model 120K).

The acetone (Sigma-Aldrich HPLC Grade 99.9% purity) was used without further purification and the compressed air (21% oxygen, 79% nitrogen) supplied by Air Liquide. The mixture compositions used are shown in Table 2.

The acetone was evaporated into the bomb, which was then closed off and the line evacuated and flushed with air prior to filling the bomb to a pressure of 1 atm with air. The line from the air supply to the bomb was kept pressurised in case of leakage during the experiment. The mixture was allowed to settle for 2–3 min while the diagnostics were readied; this settling time was a compromise between two conflicting requirements, namely the achievement of a quiescent mixture and the possibility of absorption of acetone by the bomb surfaces. The camera was set to acquire 15,000 images per second, with a total acquisition time of 72 ms and a resolution of 256 × 256 pixels. Spark ignition was achieved centrally and a video of the resulting spherical flame recorded. The bomb was allowed to cool down to room temperature between experiments and the temperature range in which the experiments were performed was thus kept constant between 22–25 °C.

Table 2
Spherical bomb mixture compositions in kPa.

Φ	Acetone	Air
0.8	4.08	95.92
0.9	4.51	95.49
1.0	4.99	95.01
1.1	5.45	94.55
1.2	5.93	94.07
1.25	6.16	93.84
1.3	6.39	93.61
1.35	6.70	93.30
1.4	6.85	93.15
1.5	7.30	92.70
1.6	7.75	92.25

The spark generated between the electrodes produces a spherical flame which expands outwardly, Fig. 3, and the flame front is typically spherical and well defined. No wrinkling of the flame is observed during its propagation indicating that the hypotheses necessary to deduce the laminar flame velocity from the measurement of the temporal evolution of the flame radius are valid [36]. The minimum radius used in determining the flame speed was 5 mm and the maximum was 35 mm; the latter corresponds to 2.2% of the total bomb volume and a pressure increase of less than 2.6%. Over this range it was possible to discriminate against the effects of ignition and of flow deformation caused by the bomb walls.

Measurement of the flame radius as a function of time from the acquired images was carried out using software especially written to provide an objective and labour-saving determination. The Matlab application [37] outputs an average value for the radius at each time, measured from the centre point between the electrodes to each pixel constituting the flame front. To take into account the asymmetry of the flame near the electrodes, an adjustable parameter was introduced, which instructs the program to ignore the flame front within a specified angle of the centre point. For *this work*, an angle of 20° above and below each electrode was chosen. A further advantage of the application is that 'noisy' images produced by the presence of particles of soot or dust on the bomb windows can be filtered out.

The observed spatial velocity was corrected for stretch in accordance [38] with Eq. (3). Integration gives Eq. (4), and thus linear regression of the radius against time data in the appropriate form yields the unstretched spatial velocity, V_S^0. This was corrected for the density gradient across the flame front by division by the ex-

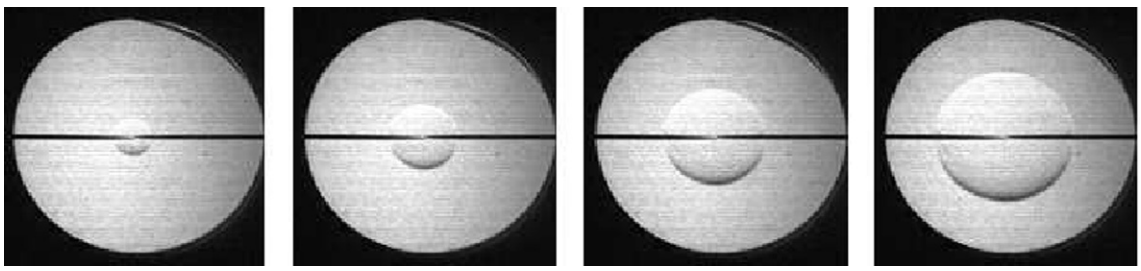

Fig. 3. Typical flame images.

pansion factor, $\sigma = \rho_u/\rho_b$, to give the unstretched laminar flame speed, S_L^0:

$$V_S = V_S^0 - L\kappa, \tag{3}$$

$$r_F - r = V_S^0(t_F - t) - 2L\ln(r_F/r) + c, \tag{4}$$

where V_S is the spatial velocity, ρ_u and ρ_b are the densities of the unburnt and burnt gas respectively, L is the Markstein length, κ is the stretch rate, r is the flame radius, r_F is the final flame radius measured, t is time and t_F is the final time measured.

As will become apparent, *vide infra*, the measured and simulated flame speeds could not be reconciled so a second set of measurements was carried out following the procedures outlined above except that a new protocol was adopted for the preparation of mixtures. This entailed using high grade anhydrous acetone (Sigma-Aldrich, Chromasolv plus for HPLC, >99.9%) with a water content of less than 0.05% by volume. All subsequent transfers of acetone liquid from the container to a storage reservoir on the bomb manifold were carried out in a glove box under an atmosphere of dry argon. Prior to filling the bomb with acetone vapour the argon blanket was pumped off.

3. Simulation

The basis of our model was a dimethyl ether mechanism [39–42] which was substantially modified to include reactions of acetone. Since our last documented model [43] a number of changes have been made to the mechanism to take into account more recent measurements of fundamental rate constants. These, and other changes, are described below. In addition a number of sub-mechanisms—those for hydrogen, carbon monoxide and methane—were re-validated but only the results for acetone and ketene are presented here. We have not included any enol chemistry in this model because of the lack of kinetic data for these newly-detected species [44].

Calculations were performed with the CHEMKIN 4.0.1 application [45]. Flame speeds were calculated with the PREMIX module which was operated with mixture-averaged transport and Soret effects. To simulate the shock tube experiments, we used the SENKIN module at constant volume. Computed ignition delays were determined from the maximum product of the concentrations of $\dot{C}_2H$ and $\dot{O}$ [34,46,47], which produces the excited species CH* via the reaction: $\dot{C}_2H + \dot{O} \rightarrow CH^* + CO$.

To validate the mechanism for acetone and the sub-mechanisms for hydrogen, carbon monoxide, methane and ketene, a series of modifications has been carried out.

The rate constant of reaction (R1), which is a very important reaction in combustion, has been updated:

$$\dot{H} + O_2 \longrightarrow \dot{O} + \dot{O}H. \tag{R1}$$

In the initial mechanism, we used the rate constant expression of Pirraglia et al. [48]. But Li et al. [49] showed that this expression over-predicts the high temperature data (above 1700 K) of Masten et al. [50], Du and Hessler [51] and Ryu et al. [52]. The analysis of Hessler [53] excluded consideration of certain sets of available elementary rate data based upon a defined uncertainty envelope. So we assumed a new rate constant of:

$$k_1 = 3.547 \times 10^{15} T^{-0.406} \exp(-8{,}359/T)\ \text{cm}^3\,\text{mol}^{-1}\,\text{s}^{-1}.$$

The effect of this change in rate constant on the overall predictive capability of the mechanism was tested by re-simulating ignition delay times and flame speed data for hydrogen oxidation [54]. It was found that no appreciable difference was observed in the model predictions.

Reaction (R24)

$$CO + \dot{O}H \longrightarrow CO_2 + \dot{H}, \tag{R24}$$

is also a very important one, because it is the main pathway for conversion of CO to CO_2. The oxidation of CO is responsible for a major fraction of the energy release derived from the oxidation of hydrocarbons. CO_2 dissociation is important in determining adiabatic flame temperatures as a function of pressure [55]. Moreover laminar flame speed predictions of hydrocarbons are strongly influenced by this reaction [56,57]. A new rate constant, for the temperature range 900–2300 K, was determined from the sum of two modified Arrhenius expressions given by Davis et al. [58], of:

$$k_{24} = 1.75 \times 10^5 \times T^{1.95} \exp(219/T)\ \text{cm}^3\,\text{mol}^{-1}\,\text{s}^{-1}.$$

The methane sub-mechanism was then validated as it is an important one in the oxidation of many hydrocarbons [59,60]. To improve the agreement between experiments and modelling, we assumed a low pressure rate constant, k_{98}^0, of $3.165 \times 10^{23} \times T^{-1.8}$ $\text{cm}^6\,\text{mol}^{-2}\,\text{s}^{-1}$, for the reaction (R98):

$$\dot{C}H_3 + \dot{H} + M \longrightarrow CH_4 + M. \tag{R98}$$

In ketene oxidation at high temperature the reaction of $CH_2 + O_2$ was very important because a large amount of CH_2 was formed. When Hidaka et al. [61] removed reaction (R136)

$$CH_2 + O_2 \longrightarrow CO_2 + \dot{H} + \dot{H} \tag{R136}$$

from their mechanism, the formation of CO_2 was much too slow and was not properly predicted. On replacing (R136) by each of these reactions in turn (R136a)–(R136e), they obtained completely incorrect profiles of CO_2 emission, even when a variety of rate expressions were used.

$$CH_2 + O_2 \longrightarrow CO + \dot{O}H + \dot{H}, \tag{R136a}$$

$$CH_2 + O_2 \longrightarrow CH_2O + \dot{O}, \tag{R136b}$$

$$CH_2 + O_2 \longrightarrow CO + H_2O, \tag{R136c}$$

$$CH_2 + O_2 \longrightarrow H\dot{C}O + \dot{O}H, \tag{R136d}$$

$$CH_2 + O_2 \longrightarrow CO_2 + H_2. \tag{R136e}$$

Similarly, when they replaced reaction (R136) by all of the reactions (R136a)–(R136e), they also obtained completely wrong profiles for CO_2. So they therefore concluded that reaction (R136) was the most important reaction between CH_2 and O_2. Thus, we decided to use only reaction (R136):

$$CH_2 + O_2 \longrightarrow CO_2 + 2\dot{H}, \tag{R136}$$

with the rate constant given by Hidaka et al. [61] of:

$$k_{136} = 2.27 \times 10^{12} \exp(-504/T)\ \text{cm}^3\,\text{mol}^{-1}\,\text{s}^{-1}.$$

The following reaction was also modified in order to obtain improved agreement:

$$CH_2CO + \dot{O}H \longrightarrow CH_2OH + CO. \tag{R230}$$

For this reaction we adopted the rate constant used by Curran et al. for their heptane mechanism [62]:

$$k_{230} = 2.0 \times 10^{12} \exp(508/T)\ \text{cm}^3\,\text{mol}^{-1}\,\text{s}^{-1}.$$

Reactions of $H\dot{C}CO$ with O_2 and $\dot{O}H$ were also modified. Improved agreement was obtained by replacing reaction (R234a) by (R234):

$$H\dot{C}CO + \dot{O}H \longrightarrow H\dot{C}O + H\dot{C}O, \tag{R234a}$$

$$H\dot{C}CO + \dot{O}H \longrightarrow CO + CO + H_2, \quad \text{(R234)}$$

and reaction (R237a) by (R237):

$$H\dot{C}CO + O_2 \longrightarrow CO_2 + H\dot{C}O, \quad \text{(R237a)}$$

$$H\dot{C}CO + O_2 \longrightarrow CO + CO + \dot{O}H, \quad \text{(R237)}$$

assuming the rate constants given by Hidaka et al. [61]: $k_{234} = 1.0 \times 10^{14}$ and $k_{237} = 4.2 \times 10^{10} \exp(-428/T)$ both in $cm^3\,mol^{-1}\,s^{-1}$, respectively.

When Hidaka et al. [61] removed reaction (R234), their data could not be successfully simulated as a consequence. For reaction (R237), Hidaka et al. [61] found that it was somewhat more suitable than reaction (R237a) for their scheme.

To improve the acetone mechanism, a number of modifications have been made. The rate of the initiation reaction (R304):

$$CH_3COCH_3 + M \longrightarrow CH_3\dot{C}O + \dot{C}H_3 + M \quad \text{(R304)}$$

is an important determinant of the concentration histories of acetone and its products [29]. Sato and Hidaka [29] used a pressure-independent rate constant of $k = 1.13 \times 10^{16} \exp(-41{,}143/T)$ $cm^3\,mol^{-1}\,s^{-1}$. To improve our simulations, a faster rate constant was required and we chose to use one that considers the effect of pressure.

The rate constant for the unimolecular decomposition of acetone was estimated using a chemical activation formulation based on Quantum Rice–Ramsperger–Kassel theory, as described by Dean [63,64]. This analysis uses a high pressure limit rate constant of $7.018 \times 10^{19} T^{-1.57} \exp(-42{,}617/T)$ s^{-1}. This rate constant was calculated from microscopic reversibility by using a rate constant of 1.0×10^{13} $cm^3\,mol^{-1}\,s^{-1}$ for $CH_3C\dot{O} + \dot{C}H_3$ addition. Our current high-pressure limit recommendation is very similar to the value of $7.244 \times 10^{25} T^{-2.72} \exp(-44{,}137/T)$ s^{-1} measured by Kiefer et al. [65], with the current value being approximately 20% faster than the Kiefer value in the temperature range of 1400–1900 K of his study. In addition, it is in very good agreement with that reported much earlier by Szwarc and Taylor [66], Clark and Pritchard [67] and Ernst and Spindler [68].

So we developed a nine parameter Troe fit:

$$k^0_{304} = 7.013 \times 10^{89} \times T^{-20.38} \exp(-53{,}959/T)\ cm^3\,mol^{-1}\,s^{-1},$$

$$k^\infty_{304} = 7.018 \times 10^{21} \times T^{-1.57} \exp(-42{,}617/T)\ s^{-1},$$

with α, T^{***}, T^* and T^{**}: 0.86, 1.0×10^{10}, 416 and 3.29×10^9.

The rate constant of reaction (R305)

$$CH_3COCH_3 + \dot{O}H \longrightarrow CH_3CO\dot{C}H_2 + H_2O \quad \text{(R305)}$$

was updated. Sato and Hidaka [29] determined a rate constant of $k = 2.00 \times 10^{13} \exp(-1{,}511/T)$ $cm^3\,mol^{-1}\,s^{-1}$, from reported values [69–71], which are rate constants for temperatures from 298 to 440 K. We decided to use very recent data determined for a larger range of temperatures. Vasudevan et al. [72] studied the reaction between $\dot{O}H$ radicals and acetone in the range 932 to 1300 K, and Yamada and Taylor [73] reported a rate constant in the temperature range 298–832 K. From these two data sets, we have determined one expression in the temperature range 298–1300 K, of:

$$k_{305} = 1.25 \times 10^5 \times T^{2.48} \exp(-224/T)\ cm^3\,mol^{-1}\,s^{-1}.$$

Reaction (R306),

$$CH_3COCH_3 + \dot{H} \longrightarrow CH_3CO\dot{C}H_2 + H_2, \quad \text{(R306)}$$

involving $\dot{H}$ abstraction from acetone, was found to be a very important one, due to the competition for H-atoms between it and reaction (1), which is the main chain-branching process at high temperatures. Using a slower rate for reaction (R306) gave a faster reactivity and in order to obtain agreement with experimental ignition delays, those predicted by the model needed to be decreased. The rate constant for reaction (R306) was therefore decreased by a factor of 3 to give:

$$k_{306} = 9.8 \times 10^5 T^{2.43} \exp(-2{,}598/T)\ cm^3\,mol^{-1}\,s^{-1}.$$

This rate constant is approximately an order of magnitude faster than that reported by Azatyan et al. [74] in the temperature range 843–928 K but is between 2.5 and 1.5 times slower than that measured by Ambidge and co-workers [75] in the temperature range 298–465 K. Interestingly, our recommended rate constant is similar to that derived by Sato and Hidaka [29], it being 30% faster than Sato and Hidaka at 1050 K, with this difference decreasing to only 2% faster at 1650 K.

Decottignies et al. [76] developed a kinetic mechanism for the oxidation of methylethylketone. We have incorporated those reactions, Table 3, given for their acetone sub-mechanism, which were absent from our mechanism. Some of these steps are quite controversial [77,78], for example:

$$CH_3COCH_3 + \dot{O}H \rightarrow CH_3\dot{C}O + CH_3OH$$

and are probably not significant under the conditions of *this work*.

Table 3
Acetone sub-mechanism [76], units: cm mol s cal.

Reactions	A	n	E
$CH_3\dot{C}O + CH_3CHO = CH_3COCH_3 + H\dot{C}O$	1.71E+11	0	0
$\dot{C}H_3 + CH_3CHO = \dot{H} + CH_3COCH_3$	1.66E+10	0	12,416
$CH_3CO\dot{C}H_2 + CH_2O = CH_3COCH_3 + H\dot{C}O$	6.31E+11	0	18,516
$CH_3CO\dot{C}H_2 + CH_3CHO = CH_3COCH_3 + CH_3\dot{C}O$	6.31E+11	0	8,516
$CH_3CO\dot{C}H_2 + C_2H_5CHO = CH_3COCH_3 + C_2H_5\dot{C}O$	3.16E+11	0	7,607
$CH_3COCH_3 + O_2 <=> CH_3\dot{C}O + CH_3\dot{O}_2$	3.00E+13	0.5	42,200
$CH_3COCH_3 + \dot{C}H_3 => \dot{C}H_3 + CH_4 + CH_2\dot{C}O$	4.00E+11	0	9,700
$CH_3COCH_3 + \dot{C}H_3 <=> CH_3\dot{C}O + C_2H_6$	7.94E+10	0	6,000
$CH_3COCH_3 + \dot{O}H <=> CH_3\dot{C}O + CH_3OH$	1.50E+12	0	0
$CH_3COCH_3 + \dot{O} <=> CH_3\dot{C}O + CH_3\dot{O}$	5.01E+12	0	1,800
$CH_3\dot{C}O + O = \dot{C}H_3 + CO_2$	1.00E+13	0	0
$CH_3\dot{C}O + \dot{O}H => \dot{C}H_3 + CO + \dot{O}H$	3.16E+13	0	0
$CH_3\dot{C}O + H\dot{O}_2 => \dot{C}H_3 + CO_2 + \dot{O}H$	3.16E+13	0	0

4. Results and discussion

Ignition delays were measured at 1.02 ± 0.03 atm, in the temperature range 1340–1930 K, at equivalence ratios of 0.5, 1 and 2 and a percentage of fuel from 1.25 to 2.5. Ignition delays become longer as the equivalence ratio is varied from 0.5 to 2, representing a decrease in reactivity with increasing equivalence ratio due to competition between acetone and oxygen for active free radicals [79]. This effect is more pronounced when the equivalence ratio is varied by adjusting the oxygen concentration, Fig. 1, than the fuel concentration, Fig. 2. This reflects the greater sensitivity of the kinetics to the oxygen concentration dependence than to that of the fuel, as can be seen from Eq. (1).

The flame speed measurements carried out at 1 atm, 298 K and in the equivalence ratio range 0.8–1.6, show a maximum at $\Phi = 1.25$ of 35.6 $cm\,s^{-1}$ for the first set of measurements whilst the second set show a similar maximum of 35.2 $cm\,s^{-1}$ but at $\Phi = 1.15$, Fig. 4. Gibbs and Calcote [32] reported a maximum flame speed, 44.4 $cm\,s^{-1}$, at an equivalence ratio, Φ, of 0.93. However, their measurements were carried out in wet air (0.31 mol% water) using a burner and were not corrected for stretch. They based their evaluation of the laminar flame speed on an averaging method in which the area of the flame is determined and the laminar flame speed derived assuming a constant speed across the total flame area. This method is well-known to be useful for rough estimations

of laminar flame speeds but not to derive accurate values. Hence the disagreement that is observed is unsurprising.

Note that previous measurements of the flame speed of dimethyl ether [80–83] compare similarly to the results of Gibbs and Calcote [32], showing a lower maximum flame speed at a higher equivalence ratio. Gibbs and Calcote [32] measured the maximum flame speed of dimethyl ether to be 48.6 $cm\,s^{-1}$ at an equivalence ratio of 0.99, whereas Gallagher [80], measured it to be 42.5 $cm\,s^{-1}$ at an equivalence ratio of 1.2, having corrected for stretch.

Likewise, the measurements of Daly et al. [82] put a lower maximum flame speed of 45.3 $cm\,s^{-1}$ at a higher equivalence ratio of 1.12 using synthetic air (20% O_2, 80% N_2) and a maximum of 46.5 $cm\,s^{-1}$ at an equivalence ratio of 1.13 using laboratory compressed air (21% O_2, 79% N_2 + Ar). The results of Qin et al. [81], obtained in a pressure-release type spherical bomb, agree with those of Daly et al. [82] except in the case of rich mixtures, where they report higher velocities. Zhao et al. [83], using particle image velocimetry and a stagnation flame burner, found the maximum flame speed to occur at a higher equivalence ratio $\Phi = 1.2$, than that determined by Gibbs and Calcote. However, their maximum flame speed of 53.3 $cm\,s^{-1}$ was much higher than that obtained by Gibbs and Calcote.

Given that the only acetone flame speed data that could be found in the literature were those of Gibbs and Calcote, it is useful to observe that the present measurements compare to them in the same way as measurements of dimethyl ether, for which there is a larger pool of experimental data.

5. Comparison of model with experiment

5.1. Ignition delays

Very good agreement is observed between experimental and computed ignition delays. When the percentage of fuel is fixed, Fig. 1, computed ignition delays are slightly faster at high temperature for the richer mixture at 2.5% oxygen. In Fig. 2, when the oxygen percentage is fixed, the model simulates the ignition delays quite well for the mixture at 1.88% fuel. When this percentage is increased (2.5%), computed ignition delays are slightly faster on the boundaries of the temperature range. But when the percentage of fuel is decreased to 1.25%, the computed ignition delays are slightly slower in the middle of the temperature range.

5.2. Flame speeds

In comparison, the agreement between simulated and experimental flame speeds is quite disappointing for the first set of measurements, Fig. 4. The model does predict the same overall shape of the curve and the same maximum flame speed, but the equivalence ratio at which this occurs does not correspond to that found experimentally. The model predicts a maximum flame speed of 35.9 $cm\,s^{-1}$ at an equivalence ratio of 1.1, whereas our experimental maximum of 35.6 $cm\,s^{-1}$ occurs at an equivalence ratio of 1.25.

The experimental procedure had been designed to avoid problems of adsorption and condensation known to be associated with ketones such as acetone [27]. The mixtures were prepared in situ and used directly rather than being allowed to sit in a mixing tank for any length of time during which loss of acetone might occur. However, it is conceivable that this propensity of acetone to be lost through adsorption may have contributed to the discrepancy between model predictions and experiment, as an assumed loss of acetone of about 12% across the range of mixtures would bring the two into very good agreement.

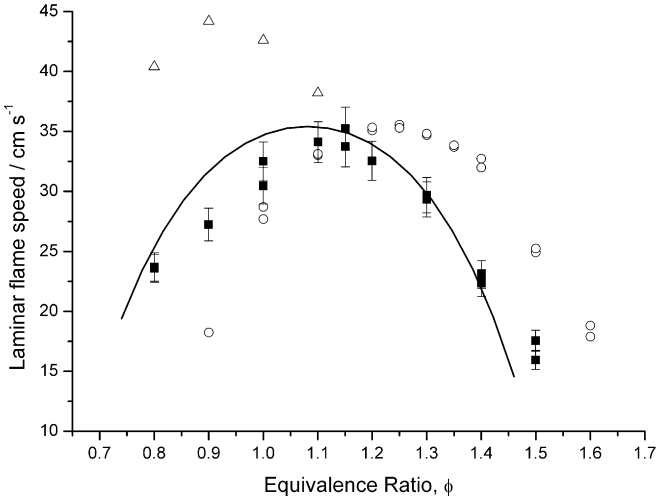

Fig. 4. Flame speeds of acetone in air at 1 atm, (■) and (○) *this work*, (△) Gibbs and Calcote [32], (—) simulation.

In an effort to improve agreement between the two, the transport options and data were varied but no improvement was observed—we succeeded in changing the maximum value of the flame speed but not the equivalence ratio at which this occurred.

It was therefore decided to re-determine the flame speeds, using an experimental procedure very similar to that previously described except that extra care was taken in the handling of anhydrous acetone by conducting all operations such as opening the sealed container under an atmosphere of argon, etc. The new experimental results are dramatically shifted with respect to the previous ones although the maximum velocity is essentially unchanged.

The agreement between simulation and experiment for this second set of measurements (arbitrarily shown with 10% error bars, Fig. 4) is now quite good and is probably capable of further improvement. It is unclear whether the apparent loss of acetone in the original set of flame speed measurements was due to surface adsorption or the presence of water vapour resulting in an incorrect equivalence ratio. An in situ non-destructive quantitative analytical system would be a decided advantage in these circumstances—such a system was not available at that time.

5.3. Induction times

We also compared induction times measured by Sato and Hidaka [29] with computed ones. They studied several mixtures with and without hydrogen. They used two methods to determine the induction time: $\tau(CO_2)$ or $\tau(OH)$, defined as the elapsed time between the reflected shock arrival and the onset of the rapid infrared emission increase for $\tau(CO_2)$ or the rapid increase of the OH absorption at 306.7 nm for $\tau(OH)$, determined from the intersection of the tangent to the curve at its inflection point with the preshock baseline.

For the computed induction times we used the profile obtained for CO_2 or OH. Fig. 5 shows that the model predicts induction times well. The agreement is very good for rich mixtures ($\Phi = 2$), such as mixtures D and F. When the oxygen percentage is fixed and the percentage of acetone increases, computed induction times become slower by a factor of about 2 at high temperature for stoichiometric mixture (mixture E), and slower by a factor of 1.5 for the entire temperature range for lean mixtures (mixture C, $\Phi = 0.5$). Fig. 6 shows that the model reproduces induction times very well for mixtures with hydrogen addition, whatever the definition of the induction time.

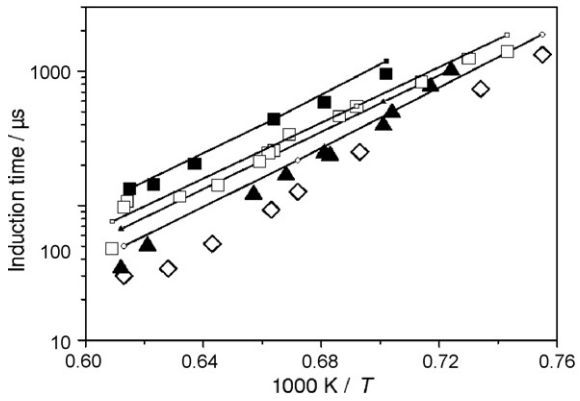

Fig. 5. Induction times τ_{CO_2} measured by Sato and Hidaka [29] of acetone:O_2:Ar mixture, (■) 1:2:97 (D), (□) 2:4:94 (F), (▲) 1:4:95 (E) and (◇) 0.5:4.0:95.5 (C), (−) simulation.

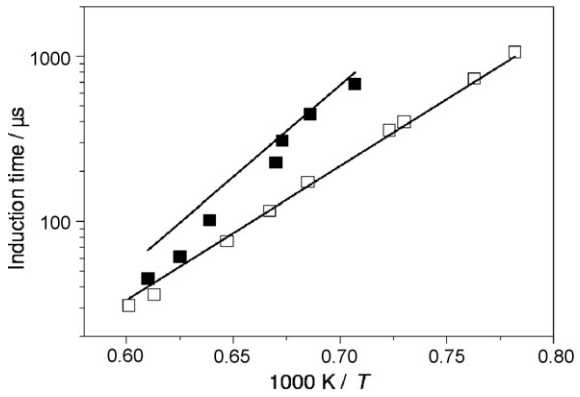

Fig. 6. Induction times measured by Sato and Hidaka [29] of acetone:H_2:O_2:Ar mixture, τ_{CO_2} (■) 1:2:2:95 (H), τ_{OH} (□) 0.1:2.0:2.0:95.0 (G), (−) simulation.

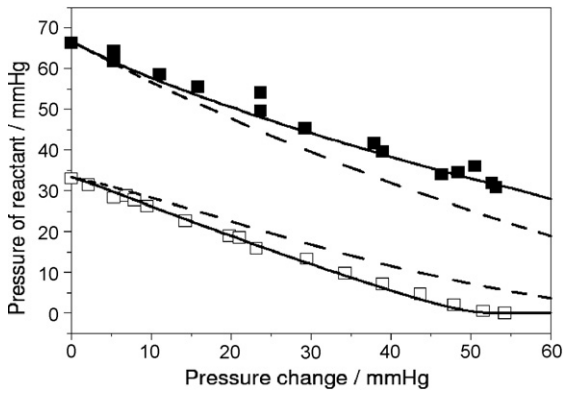

Fig. 7. Consumption of reactants at 771 K with initial mixture of 66.7 mmHg acetone (■) and 33.3 mmHg oxygen (□) [25], (---) mechanism with (R406), (R413), (R414), (−) mechanism without (R406), (R413), (R414).

5.4. Static reactor

To extend the validation range, we also compared our mechanism against the experimental results of Barnard and Honeyman [25] where acetone oxidation was studied in a conventional static reactor at 771 K. Fig. 7 gives pressure of reactants (acetone and oxygen) against pressure change (ΔP), defined as $\Delta P = P_{t=0} - P_t$, for an initial mixture of 66.6 Torr of acetone and 33.3 Torr of oxygen. It can be seen that the results obtained with the initial mechanism do not simulate acetone and oxygen profiles that well. A sensitivity study for acetone showed that three reactions are very important for acetone consumption:

$$CH_3\dot{C}O + CH_3CHO \longrightarrow CH_3COCH_3 + H\dot{C}O, \quad \text{(R406)}$$

$$CH_3COCH_3 + \dot{C}H_3 \longrightarrow CH_3\dot{C}O + C_2H_6, \quad \text{(R413)}$$

$$CH_3COCH_3 + \dot{O}H \longrightarrow CH_3\dot{C}O + CH_3OH. \quad \text{(R414)}$$

These three reactions have been adopted from the sub-mechanism for acetone given by Decottignies et al. [76] who assumed the rate constant of Gill et al. [84] for (R406) and rate constants measured in their laboratory for (R413) and (R414) [85]. These reactions are not elementary and are unlikely to be significant channels under our conditions and therefore they were deleted from our mechanism. It can be seen in Fig. 7 that when these three reactions were removed, the model simulates the experimental data of Barnard et Honeyman [25] quite well but crucially did not change our simulated results for ignition delays and flame speeds.

The final mechanism, AcetOne, consists of 416 reactions and 81 species, and is freely available in Chemkin format at http://c3.nuigalway.ie/.

5.5. Flame species profiles

Successful simulation of the low-pressure premixed flame speciation data by the Qi group [31] is crucially dependent upon a good estimate of the flame temperature as a function of the height above the burner. Using the published temperature profiles resulted [86] in very poor agreement with experiment; the authors state that for modelling purposes their published temperature profiles should be lowered by 100 K in the burnt gas region. This arises because the cooling effect of the sampling probe can be considerable, for example, they quote the work by Desgroux et al. [87] on low-pressure premixed methanol–air flames who reported 100 K cooling in the burnt gas zone of their 6 cm burner. Although not explicitly stated these latter authors present evidence for temperature drops of >240 K in the reaction zone.

Lowering the flame temperature uniformly by 100 K or more had very little effect on the simulated acetone concentration profile—the agreement with experiment remained very poor—and this was still the case when we replaced the existing C1–C3 sub-mechanism in AcetOne with the very latest, and as yet unpublished, version of our ongoing studies. Hence we concluded that more drastic changes of the temperature profiles were required—subject of course to the fact that our acetone model is not complete, lacking as it does any enol chemistry. Therefore a number of different, wholly artificial, temperature profiles were drawn up for exploratory purposes, based on the equation:

$$T(z) = T_i + \left[(T_f - T_i)\exp(-\alpha/z)\right], \quad (5)$$

where z is the height above the burner, T_i is the initial flame temperature at burner height $z = 0$, T_f is the final burnt gas temperature and α is a constant. The effects of adopting such temperature profiles are quite dramatic; for example, see Fig. 8 for results based on the published profile and that produced from (5) with $\alpha = 2.3$, $T_i = 400$ and $T_f = 1900$ K for the major species acetone, O_2, H_2O, CO, CO_2 and H_2.

As regards some of the minor species such as formaldehyde, ketene, ethene and methyl radical the same artificial temperature profile as that outlined above gives much better agreement with experiment for the rich flame than the published temperature profile, Fig. 9. The same conclusions may be drawn from an inspection of mole fraction versus height above the burner plots for the major (not shown here) and minor species, Fig. 10, in the lean flame—note that no attempt was made to fit a different artificial temperature profile for the hotter lean flame.

Finally we curve-fitted the temperature data of Desgroux et al. obtained with the sampling probe in place and with the probe

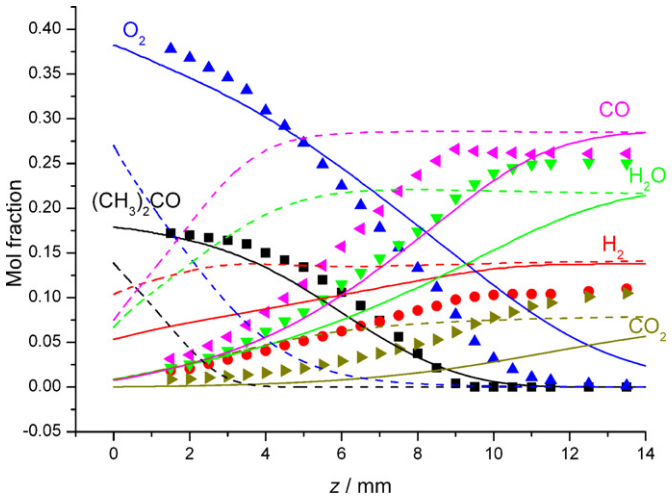

Fig. 8. Effect of temperature profiles on major species mole fractions as a function of height above the burner for a rich acetone flame [31]; (---) published, (—) artificial.

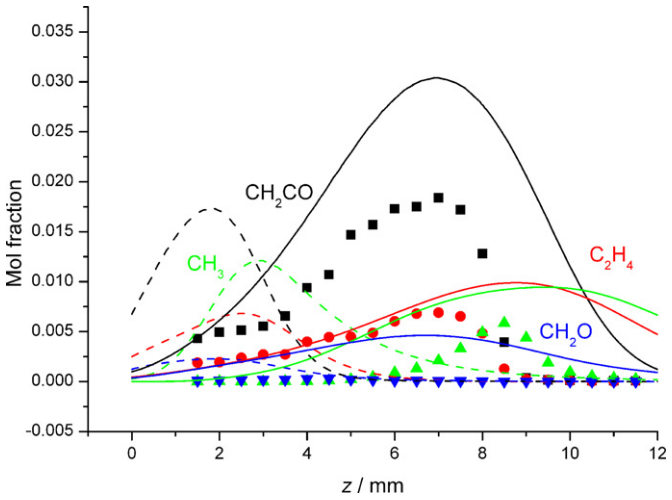

Fig. 9. Effect of temperature profiles on some minor species mole fractions as a function of height above the burner for a rich acetone flame [31]; (---) published, (—) artificial.

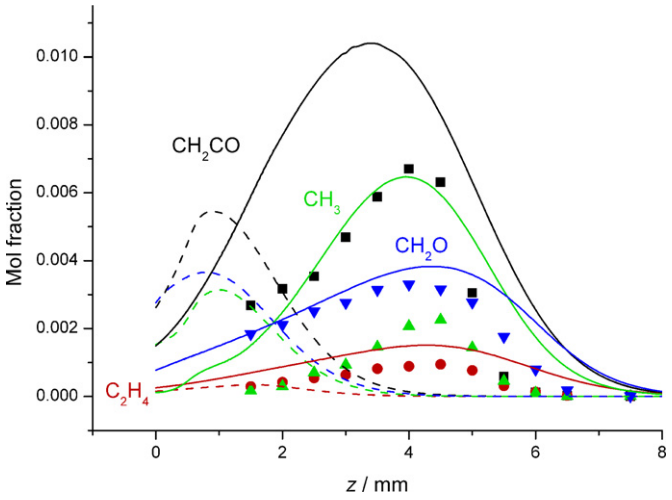

Fig. 10. Effect of temperature profiles on some minor species mole fractions as a function of height above the burner for a lean acetone flame [31]; (---) published, (—) artificial.

withdrawn (as shown in their Fig. 4) to generate temperature differences as a function of the height above the burner and corrected the published Qi temperature profiles by these differences. Exactly how transferable this procedure is clearly open to question but this resulted in very poor agreement with experiment. It appears that more drastic temperature corrections apply to the molecular-beam sampling photoionisation mass spectrometric apparatus than can be inferred from the Desgroux et al. work [87].

6. Sensitivity analysis

Sensitivity studies of acetone ignition delay and flame speed data are shown in Figs. 11 and 12, respectively. It can be seen that the most important reaction, for the two sensitivity studies performed, is reaction (R1)

$$\dot{H} + O_2 \longrightarrow \dot{O} + \dot{O}H. \quad (R1)$$

For the ignition delay, Fig. 11 shows that the reactions involving acetone are important, such as reactions (R304), (R305), (R306) and also reaction (R411)

$$CH_3COCH_3 + O_2 \longrightarrow CH_3\dot{C}O + CH_3\dot{O}_2. \quad (R411)$$

For the flame speed, Fig. 12, none of the reactions involving acetone have an important sensitivity coefficient. The most important reactions are (R26), (R8), (R98) and (R24):

$$H\dot{C}O + M \longrightarrow \dot{H} + CO + M, \quad (R26)$$

$$H_2O + M \longrightarrow \dot{H} + \dot{O}H + M, \quad (R8)$$

$$\dot{C}H_3 + \dot{H} + M \longrightarrow CH_4 + M, \quad (R98)$$

$$CO + \dot{O}H \longrightarrow CO_2 + \dot{O}H. \quad (R24)$$

These reactions are very sensitive to the flame speed calculations of hydrogen, carbon monoxide and methane [49,54,55,88]. The agreement between our simulations and flame speeds measured for H_2/air, H_2/O_2/He, CO/H_2/air and CH_4/air are very good.

A sensitivity study showed that the acetone is essentially consumed by three reactions forming methyl radicals (R304) or the radicals $CH_3C\dot{O}CH_2$ (R305) and (R306):

$$36\% \quad CH_3COCH_3 + M \longrightarrow CH_3\dot{C}O + \dot{C}H_3 + M, \quad (R304)$$

$$31\% \quad CH_3COCH_3 + \dot{H} \longrightarrow CH_3C\dot{O}CH_2 + H_2, \quad (R306)$$

$$16\% \quad CH_3COCH_3 + \dot{O}H \longrightarrow CH_3C\dot{O}CH_2 + H_2O. \quad (R305)$$

Thereafter the acetyl radical $CH_3\dot{C}O$ decomposes via reaction (R210), forming a methyl radical and carbon monoxide:

$$CH_3\dot{C}O + M \longrightarrow \dot{C}H_3 + \dot{C}O + M. \quad (R210)$$

The radical $CH_3C\dot{O}CH_2$ produced by reactions (R305) and (R306) plays an important role in ketene formation, via (R313):

$$CH_3C\dot{O}CH_2 \longrightarrow CH_2CO + \dot{C}H_3. \quad (R313)$$

Ketene is also consumed in different ways, producing methyl radicals $\dot{C}H_3$ (R225), hydroxymethyl radicals $\dot{C}H_2OH$ (R230) and mainly ethynyloxy radicals $H\dot{C}CO$ ((R226) and (R229)):

$$54\% \quad CH_2CO + \dot{H} \longrightarrow H\dot{C}CO + H_2, \quad (R226)$$

$$19\% \quad CH_2CO + \dot{H} \longrightarrow \dot{C}H_3 + CO, \quad (R225)$$

$$15\% \quad CH_2CO + \dot{O}H \longrightarrow H\dot{C}CO + H_2O, \quad (R229)$$

$$8\% \quad CH_2CO + \dot{O}H \longrightarrow \dot{C}H_2OH + CO. \quad (R230)$$

$H\dot{C}CO$ is consumed in four main reactions (R232), (R233), (R234) and (R235):

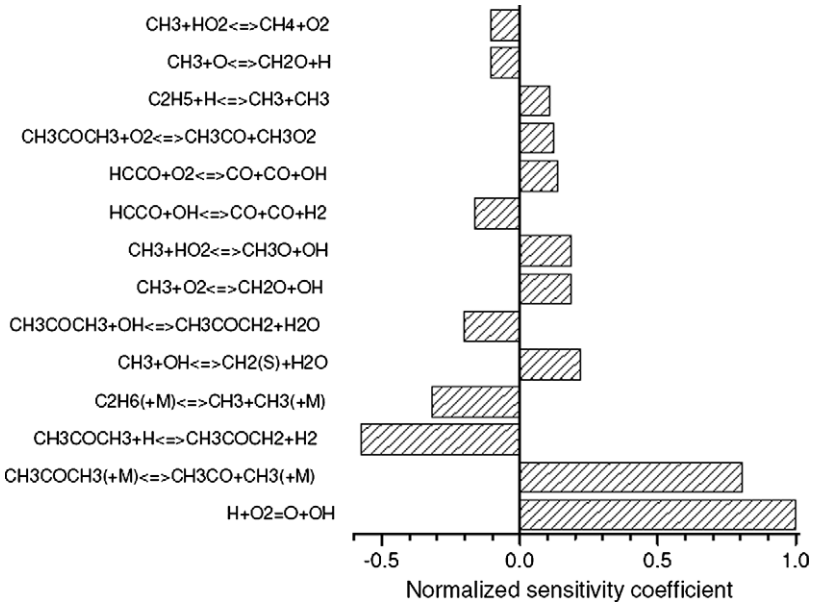

Fig. 11. Sensitivity study of ignition delay of acetone:O_2:Ar = 1.25:5:93.75 at 1470 K and 1 atm.

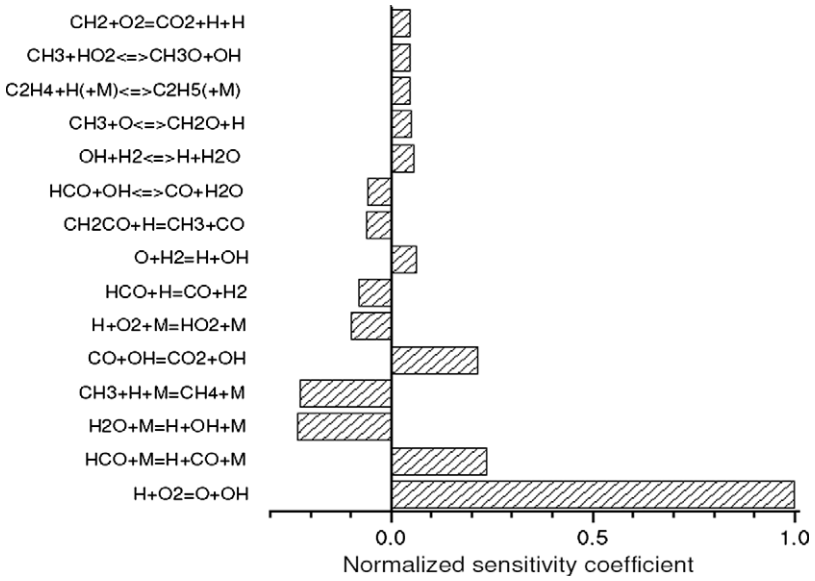

Fig. 12. Sensitivity study of acetone/air flame speed at 298 K and 1 atm.

49% $H\dot{C}CO + O_2 \longrightarrow CO + CO + \dot{O}H$, (R235)

34% $H\dot{C}CO + \dot{O}H \longrightarrow CO + CO + H_2$, (R232)

10% $H\dot{C}CO + \dot{O} \longrightarrow CO + CO + \dot{H}$, (R234)

7% $H\dot{C}CO + \dot{H} \longrightarrow CH_2(S) + CO$. (R233)

Many reactions (R210), (R225), (R304), (R313) produce $\dot{C}H_3$, which leads primarily (56%) to the production of ethane via (R149)

$\dot{C}H_3 + \dot{C}H_3 + M \longrightarrow C_2H_6 + M$. (R149)

Hydroxymethyl radical $\dot{C}H_2OH$, formed via (R230), is mainly consumed (93%) via reaction with molecular oxygen (R72)

$CH_2OH + O_2 \longrightarrow CH_2O + H\dot{O}_2$. (R72)

This study is illustrated in Fig. 13. When acetone decomposes, the first product is $\dot{C}H_3$ (R210), (R304) and (R313), which results in the production of ethane (R149). The decomposition of acetonyl, formed via reactions (R305) and (R306), leads principally to the

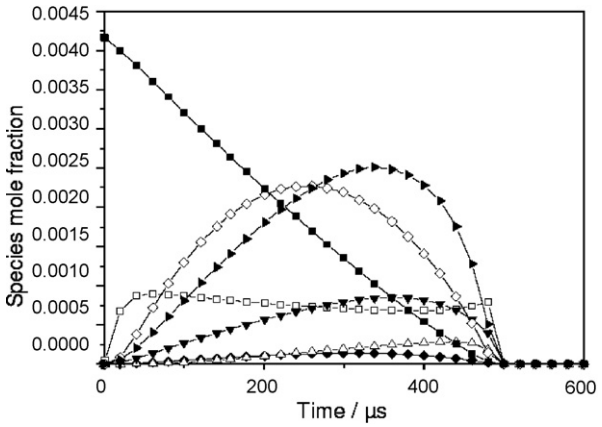

Fig. 13. Computed species histories obtained for acetone:O_2:Ar = 1.25:5:93.75 at 1470 K and 1 atm, (■) CH_3COCH_3/3, (▶) CH_2CO, (◆) CH_3OH, (▼) CH_2O, (△) HCCO, (□) CH_3, (◇) C_2H_6.

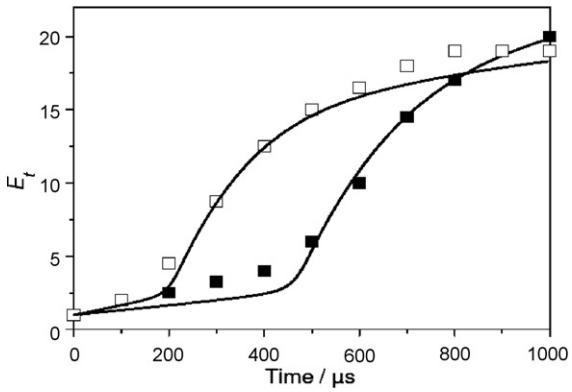

Fig. 14. Comparison of the profiles E_t observed at 4.24 μm [61] with the calculated ones at (■) 1686 K and (□) 1797 K, using mixture ketene:O_2:Ar = 0.26:0.52:99.22.

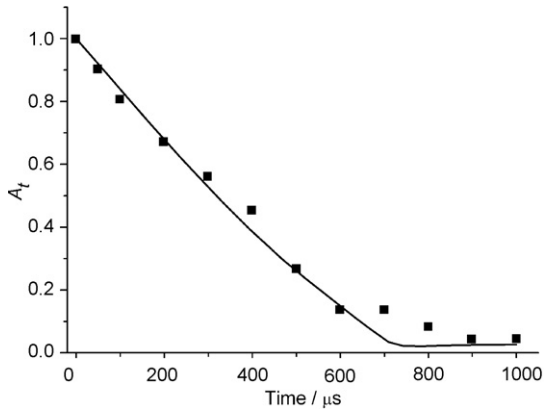

Fig. 15. Comparison of the observed UV-absorption curve A_t at 200 nm [61] with the calculated ones at 1633 K using mixture ketene:O_2:Ar = 0.26:0.52:99.22.

formation of ketene (R313). Then ketene goes on to form HĊCO (R226) and (R229) and CH_2OH (R230), which in turn produces CH_2O (R72).

7. Ketene

This study showed that ketene is a very important species in the oxidation of acetone. We therefore decided to also validate our mechanism for this species using the data given by Hidaka et al. [61]. They studied ketene oxidation behind reflected shock waves at 1050–2050 K at total pressures between 1.1 and 3.0 atm. They followed ketene decay and carbon dioxide production using UV-absorption at 200 nm and time-resolved IR-emission at 4.24 μm, respectively.

The model reproduces the ketene data well, Figs. 14, 15 and 16. E_t in Fig. 14 was defined as $E_t = E/E_0$ where E_0 and E are the signal voltages corresponding to the emission intensity at the reflected shock front ($t = 0$) and at time t, respectively. The IR-emission at 4.24 μm comes not only from carbon dioxide, but also from ketene and carbon monoxide. The authors give relationships between the emission intensity and temperature for CO_2, CO and CH_2CO. A_t in Figs. 15 and 16 was defined as $A_t = \log(I_f/I_t)/\log(I_f/I_0)$ where I_f is the signal voltage corresponding to the full intensity and I_0 and I_t are the signal voltages corresponding to the absorption intensity at the reflected shock front ($t = 0$) and at time t, respectively. Absorption at 200 nm is due to many species: CH_2CO, CO_2, O_2, C_2H_4, C_2H_2—but the authors quote equations between the total absorption data A_t and temperature for each of the above-mentioned species.

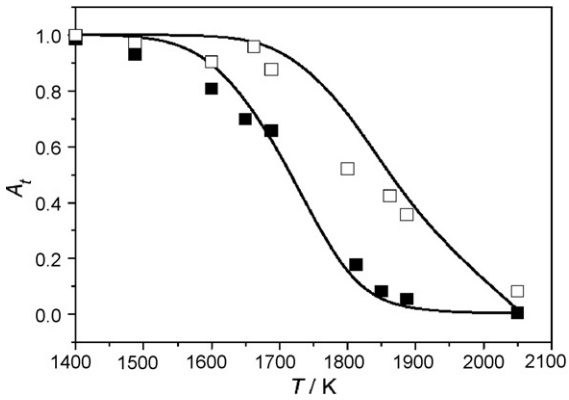

Fig. 16. Relationship between absorption data A_t and temperature T [61]; mixture ketene:O_2:Ar = 0.26:0.14:99.6, observed at (□) 50 μs and (■) 200 μs.

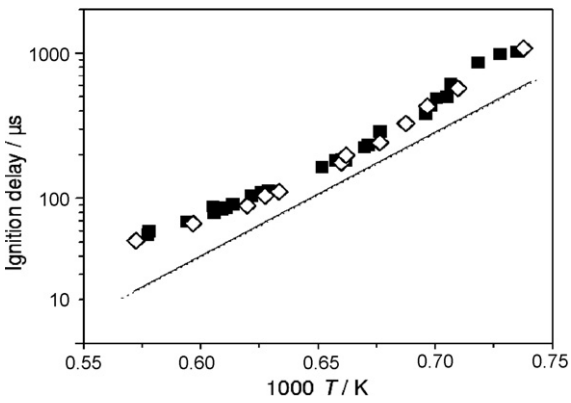

Fig. 17. Ignition delays measured for heptane:acetone:O_2:Ar mixture at 1 atm experiments: (■) 0.4:0:4.4:95.2 and (◇) 0.34:0.06:4.4:95.2; simulation: (—) 0.4:0:4.4:95.2 and (···) 0.34:0.06:4.4:95.2.

8. Effect of acetone on *n*-heptane

Since engine visualisation or imaging studies rarely use a pure fuel tracer, but rather a 10–15% blend of fuel and tracer, we have investigated the effect that the addition of acetone has on a typical fuel, *n*-heptane. We compared ignition delay times measured for a stoichiometric mixture containing 0.4% heptane with one where 15% of the heptane has been replaced by acetone. Fig. 17 shows that there is no observable effect when acetone is added to the heptane mixture. The simulation gives the same result, there is no difference between ignition delays calculated for heptane mixture with or without acetone. For these calculations, we added the acetone sub-mechanism to the heptane mechanism [35].

Zhang et al. [89] examined the impact on combustion performance of adding other widely used fuel tracers, 3-pentanone and toluene, to iso-octane by measuring a number of parameters in a spark-ignited gasoline engine, such as peak pressure, location of peak pressure, indicated mean effective pressure and peak burn rate. They found the effect to be minor and mostly statistically insignificant which is in concordance with our results for acetone-doped *n*-heptane ignition delays.

9. Conclusions

Shock tube ignition delay measurements of acetone at 1 atm, at temperatures from 1340 to 1930 K and a range of equivalence ratios have been presented. Flame speed measurements in a spherical bomb have been carried out at 1 atm, near 298 K and a range of equivalence ratios; the pitfalls associated with handling acetone are highlighted.

A detailed chemical kinetic model validated for sub-mechanisms for hydrogen, carbon monoxide, methane and ketene has been

used to simulate a range of experimental data, showing good agreement in general. It is probable that substantive temperature corrections to measured flame temperature profiles are required for successful modelling of species concentrations as a function of height above the burner.

It is demonstrated that the addition of up to 15% acetone to an *n*-heptane stoichiometric mixture has no effect as regards the ignition delay time.

Acknowledgments

G.B. thanks the Irish Research Council for Science, Engineering and Technology for an Embark Fellowship. S.P. thanks the EU for a Marie Curie Fellowship, ENK6-CT2002-50516. Funding from an EU Marie Curie Transfer of Knowledge grant (MKTD-CT-2004-517248) is acknowledged.

References

[1] A. Lozano, B. Yip, R.K. Hanson, Exp. Fluids 13 (1992) 369–376.
[2] R.K. Hanson, J.M. Seitzman, P.H. Paul, Appl. Phys. B 50 (1990) 441–454.
[3] A. Lozano, S.H. Smith, M.G. Mungal, R.K. Hanson, AIAA J. 32 (1993) 218–221.
[4] D. Wolff, H. Schluter, V. Beushausen, P. Andresen, Ber. Bunsen-Ges. Phys. Chem. 97 (1993) 1738–1741.
[5] M.C. Thurber, F. Grisch, R.K. Hanson, Opt. Lett. 22 (1997) 251–253.
[6] S. Einecke, C. Schulz, V. Sick, Appl. Phys. B 71 (2000) 717–723.
[7] M.C. Thurber, R.K. Hanson, Exp. Fluids 30 (2001) 93–101.
[8] C. Schulz, V. Sick, Prog. Energ. Combust. 31 (2005) 75–121.
[9] V. Robin, A. Mura, M. Champion, O. Degardin, B. Renou, M. Boukhalfa, Combust. Flame 153 (2008) 288–315.
[10] M.C. Thurber, F. Grisch, B.J. Kirby, M. Votsmeier, R.K. Hanson, Appl. Opt. 37 (1998) 4963–4978.
[11] M.C. Thurber, R.K. Hanson, Appl. Phys. B 69 (1999) 229–240.
[12] A. Braeuer, F. Beyrau, A. Leipertz, Appl. Opt. 45 (2006) 4982–4989.
[13] W. Koban, J.D. Koch, V. Sick, N. Wermuth, R.K. Hanson, C. Schulz, Proc. Combust. Inst. 30 (2005) 1545–1553.
[14] C. Maqua, V. Depredurand, G. Castanet, M. Wolff, F. Lemoine, Exp. Fluids 43 (2007) 979–992.
[15] H. Seyfried, J. Olofsson, J. Sjoeholm, M. Richter, M. Alden, A. Vressner, A. Hultqvist, B. Johansson, SAE 2007, SP-2100, pp. 429–437.
[16] O. Dégardin, B. Renou, A. Boukhalfa, Exp. Fluids 40 (2006) 452–463.
[17] H.B. Singh, D. O'Hara, D. Herlth, W. Sachse, D.R. Blake, J.D. Bradshaw, M. Kanakidou, P.J. Crutzen, J. Geophys. Res. Atmos. 99 (1994) 1805–1819.
[18] M. Yujing, A. Mellouki, J. Photochem. Photobiol. A 134 (2000) 31–36.
[19] H. Singh, Y. Chen, A. Staudt, D. Jacob, D. Blake, B. Heikes, J. Snow, Nature 410 (2001) 1078–1081.
[20] M. Szewczynska, E. Dobrzynska, M. Posniak, Chem. Anal. 53 (2008) 59–70.
[21] A.M. El-Nahas, J.M. Simmie, M.V. Navarro, J.W. Bozzelli, G. Black, H.J. Curran, Phys. Chem. Chem. Phys. (2008), doi:10.1039/b810853f.
[22] D.E. Hoare, T.M. Li, Combust. Flame 12 (1968) 136–144.
[23] D.E. Hoare, T.M. Li, Combust. Flame 12 (1968) 145–154.
[24] D.E. Hoare, D.E. Lill, J. Chem. Soc. Faraday Trans. I 69 (1973) 603–610.
[25] J.A. Barnard, T.W. Honeyman, Proc. R. Soc. London Ser. A 279 (1964) 236–247.
[26] J.A. Barnard, T.W. Honeyman, Proc. R. Soc. London Ser. A 279 (1964) 248–259.
[27] T. Tsuboi, K. Ishii, S. Tamura, Nippon Kikai Gakkai Ronbunshu, B hen 67 (2001) 2797–2804.
[28] A.M. El-Nahas, J.W. Bozzelli, J.M. Simmie, M.V. Navarro, G. Black, H.J. Curran, J. Phys. Chem. A 110 (2006) 13618–13623.
[29] K. Sato, Y. Hidaka, Combust. Flame 122 (2000) 291–311.
[30] M. Chaos, Z. Zhao, A. Kazakov, F.L. Dryer, in: 31st Int. Symp. on Combust., Heidelberg (2006), work-in-progress poster.
[31] Y. Li, L. Wei, Z. Tian, B. Yang, J. Wang, T. Zhang, F. Qi, Combust. Flame 152 (2008) 336–359.
[32] G.J. Gibbs, H.F. Calcote, J. Chem. Eng. Data 3 (1959) 226–235.
[33] Morley, Gaseq v0.76, http://www.gasEq.co.uk.
[34] D.C. Horning, D.F. Davidson, R.K. Hanson, J. Propul. Power 18 (2002) 363–371.
[35] J.M. Smith, J.M. Simmie, H.J. Curran, Int. J. Chem. Kinet. 37 (2005) 728–736.
[36] N. Lamoureux, N. Djebaïli-Chaumeix, C.-E. Paillard, Exp. Therm. Fluid Sci. 27 (2003) 385–393.
[37] c3.nuigalway.ie/software.html.
[38] N. Lamoureux, N. Djebaïli-Chaumeix, C.E. Paillard, J. Phys. IV Fr. 12 (2002) 445–452.
[39] H.J. Curran, W.J. Pitz, C.K. Westbrook, P. Dagaut, J.C. Boettner, M. Cathonnet, Int. J. Chem. Kinet. 30 (1998) 229–241.
[40] S.L. Fischer, F.L. Dryer, H. J Curran, Int. J. Chem. Kinet. 32 (2000) 713–740.
[41] H.J. Curran, S.L. Fischer, F.L. Dryer, Int. J. Chem. Kinet. 32 (2000) 741–759.
[42] E.W. Kaiser, T.J. Wallington, M.D. Hurley, J. Platz, H.J. Curran, W.J. Pitz, C.K. Westbrook, J. Phys. Chem. A 104 (2000) 8194–8206.
[43] X.L. Zheng, T.F. Lu, C.K. Law, C.K. Westbrook, H.J. Curran, Proc. Combust. Inst. 30 (2005) 1101–1109.
[44] T.A. Cool, K. Nakajima, T.A. Mostefaoui, F. Qi, A. McIlroy, P.R. Westmoreland, M.E. Law, L. Poisson, D.S. Peterka, M. Ahmed, J. Chem. Phys. 119 (2003) 8356–8365.
[45] R.J. Kee, F.M. Rupley, J.A. Miller, M.E. Coltrin, J.F. Grcar, E. Meeks, H.K. Moffat, A.E. Lutz, G. Dixon-Lewis, M.D. Smooke, J. Warnatz, G.H. Evans, R.S. Larson, R.E. Mitchell, L.R. Petzold, W.C. Reynolds, M. Caracotsios, W.E. Stewart, P. Glarborg, C. Wang, O. Adigun, W.G. Houf, C.P. Chou, S.F. Miller, P. Ho, D.J. Young, CHEMKIN Release 4.0, Reaction Design, Inc., San Diego, CA (2004).
[46] D.F. Davidson, J.T. Herbon, D.C. Horning, R.K. Hanson, Int. J. Chem. Kinet. 33 (2001) 775–783.
[47] K.T. Walsh, M.B. Long, M.A. Tanoff, M.D. Smooke, Proc. Combust. Inst. 27 (1998) 615–623.
[48] A.N. Pirraglia, J.V. Michael, J.W. Sutherland, R.B. Klemm, J. Phys. Chem. 93 (1989) 282–291.
[49] J. Li, Z. Zhao, A. Kazakov, F.L. Dryer, Int. J. Chem. Kinet. 36 (2004) 1–10.
[50] D.A. Masten, R.K. Hanson, C.T. Bowman, J. Phys. Chem. 94 (1990) 7119–7128.
[51] H. Du, J.P. Hessler, J. Chem. Phys. 96 (1992) 1077–1092.
[52] S.O. Ryu, S.M. Hwang, M.J. Rabinowitz, J. Phys. Chem. 99 (1995) 13984–13991.
[53] J.P. Hessler, J. Phys. Chem. A 102 (1998) 4517–4526.
[54] M.S. O'Conaire, Ph.D. thesis, National University of Ireland, Galway, 2005.
[55] J. Li, Z. Zhao, A. Kazakov, M. Chaos, F.L. Dryer, J.J. Scire Jr., Int. J. Chem. Kinet. 39 (2007) 109–136.
[56] J. Warnatz, in: W.C. Gardiner Jr. (Ed.), Combustion Chemistry, Springer-Verlag, New York, 1984.
[57] J.A. Miller, R.J. Kee, C.K. Westbrook, Annu. Rev. Phys. Chem. 41 (1990) 345–387.
[58] S.G. Davis, A.V. Joshi, H. Wang, F. Egolfopoulos, Proc. Combust. Inst. 30 (2005) 1283–1292.
[59] J.M. Simmie, Prog. Energy Combust. Sci. 29 (2003) 599–634.
[60] P. Dagaut, J.C. Boettner, M. Cathonnet, Combust. Sci. Technol. 77 (1991) 127–148.
[61] Y. Hidaka, K. Kimura, K. Hattori, T. Okuno, Combust. Flame 106 (1996) 155–167.
[62] H.J. Curran, P. Gaffuri, W.J. Pitz, C.K. Westbrook, Combust. Flame 114 (1998) 149–177.
[63] A.M. Dean, J. Phys. Chem. 89 (1985) 4600–4608.
[64] A.M. Dean, J.M. Bozzelli, E.R. Ritter, Combust. Sci. Technol. 80 (1991) 63–85.
[65] S. Saxena, J.H. Kiefer, S.J. Klippenstein, Proc. Combust. Inst. (2008), doi:10.1016/j.proci.2008.05.032.
[66] M. Szwarc, J.W. Taylor, J. Chem. Phys. 23 (1955) 2310–2314.
[67] D. Clark, H.O. Pritchard, J. Chem. Soc. London (1956) 2136–2140.
[68] J. Ernst, K. Spindler, Ber. Bunsen-Ges. Phys. Chem. 79 (1975) 1163–1168.
[69] T.J. Wallington, M.J. Kurylo, J. Phys. Chem. 91 (1987) 5050–5054.
[70] C. Chiorboli, C.A. Bignozzi, A. Maldotti, P.F. Giardini, A. Rossi, V. Carassiti, Int. J. Chem. Kinet. 15 (1983) 579–586.
[71] R. Atkinson, D.L. Baulch, R.A. Cox, R.F. Hampson, J.A. Kerr, J. Troe, J. Phys. Chem. Ref. Data 18 (1989) 881–1097.
[72] V. Vasudevan, D.F. Davidson, R.K. Hanson, J. Phys. Chem. A 109 (2005) 3352–3359.
[73] T. Yamada, P.H. Taylor, A. Goumri, P. Marshall, J. Chem. Phys. 119 (2003) 10600–10606.
[74] V.V. Azatyan, Zh.Kh. Gyulbekyan, A.B. Nalbandyan, L.B. Romanovich, Arm. Khim. Zh. 25 (1972) 727–731.
[75] P.F. Ambidge, J.N. Bradley, D.A. Whytock, J. Chem. Soc. Faraday Trans. I 72 (1976) 1870–1876.
[76] V. Decottignies, L. Gasnot, J.F. Pauwels, Combust. Flame 130 (2002) 225–240.
[77] L. Masgrau, A. González-Lafont, J.M. Lluch, J. Phys. Chem. A 106 (2002) 11760–11770.
[78] J.D. Raff, P.S. Stevens, R.A. Hites, J. Phys. Chem. A 109 (2005) 4728–4735.
[79] G. Ben-Dor, O. Igra, T. Elperin, A. Lifshitz (Eds.), Handbook of Shock Waves, vol. 3, Academic Press, New York, 2001, pp. 233–255.
[80] S.M. Gallagher, Ph.D. thesis, National University of Ireland, Galway, 2003.
[81] X. Qin, Y. Ju, Proc. Combust. Inst. 30 (2005) 233–240.
[82] C.A. Daly, J.M. Simmie, J. Würmel, N. Djebaïli, C. Paillard, Combust. Flame 125 (2001) 1329–1340.
[83] Z. Zhao, A. Kazakov, F.L. Dryer, Combust. Flame 139 (2004) 52–60.
[84] R.J. Gill, W.D. Johnson, G.H. Atkinson, Chem. Phys. 58 (1981) 29–44.
[85] M. Kayele, Ph.D. thesis, Université des Sciences et Technologies de Lille, France, 1993.
[86] For these calculations we used ChemkinPro from Reaction Design.
[87] P. Desgroux, L. Gasnot, J.F. Pauwels, L.R. Sochet, Appl. Phys. B 61 (1995) 401–407.
[88] K.J. Hughes, T. Turanyi, A.R. Clague, M.J. Pilling, Int. J. Chem. Kinet. 33 (2001) 513–538.
[89] R. Zhang, N. Wermuth, V. Sick, SAE 2004-01-2975.